The influence of the cloud shell on bulk tracer measurements of LES cloud entrainment

Jordan T Dawe * and Philip H Austin

Department of Earth and Ocean Sciences, University of British Columbia, Vancouver, BC, Canada.

* *Corresponding author address:* Jordan T Dawe, Department of Earth and Ocean Sciences, University of British Columbia, 6339 Stores Road, Vancouver, BC, V6T 1Z4, Canada.

E-mail: jdawe@eos.ubc.ca

ABSTRACT

Direct measurements of entrainment and detrainment rates from LES model cloud fields produce values twice as large as those produced from bulk conserved tracer budget calculations. This difference can be explained by three effects: the presence of a shell of moist air around the clouds, Reynolds correlations between entrainment rates and tracer values, and numerical errors in the calculation methods. Correlations between the vertical momentum and the entrainment rate create strong vertical momentum Reynolds fluxes, making the assumption that clouds entrain fluid with zero vertical momentum incorrect. Variability in the properties of the moist cloud shell has strong impacts on entrainment values inferred from bulk tracer calculations. These results indicate the dynamics of the cloud shell should be included in parameterizations of cumulus clouds used in general circulation models.

1. Introduction

The rate at which air is entrained into and detrained from clouds affects cloud properties, cloud top height, and vertical transports of heat and moisture. Proper simulation of these subgrid-scale effects in General Circulation Models (GCM) depends on the accurate parameterization of entrainment and detrainment (Bechtold et al. 2008; Rougier et al. 2009; de Rooy and Siebesma 2010).

Large Eddy Simulation (LES) is a primary tool used to study these dynamics. LES entrainment and detrainment rates are typically calculated using budgets of bulk conserved tracer variables to inferring the amount of fluid exchange between the clouds and the surrounding air. These rates are then used in simple entraining plume parameterizations to

evaluate sub-grid scale cloud transports. Siebesma and Cuijpers (1995) derive the following equations for entrainment and detrainment from a cloud core plume, where cloud core is defined as regions having condensed liquid water, positive buoyancy, and upward vertical velocity:

$$E_\phi(\phi_c - \phi_e) = -M_c\frac{\partial\phi_c}{\partial z} - \frac{\partial\rho a\overline{w'\phi'}^c}{\partial z} - \rho a\frac{\partial\phi_c}{\partial t} + a\rho\left(\frac{\partial\bar{\phi}}{\partial t}\right)_{forcing} \tag{1}$$

and

$$D_\phi(\phi_c - \phi_e) = -M_c\frac{\partial\phi_e}{\partial z} + \frac{\partial\rho(1-a)\overline{w'\phi'}^e}{\partial z} + \rho(1-a)\frac{\partial\phi_e}{\partial t} - \rho(1-a)\left(\frac{\partial\bar{\phi}}{\partial t}\right)_{forcing} \tag{2}$$

Here ϕ represents any conserved bulk tracer, such as the total specific humidity q_t (kg water kg^{-1} moist air) or the liquid-water moist static energy h (J kg^{-1}), a is the fractional cloud core area, ρ is the density of the air in kg m^{-3}, M_c is vertical cloud core mass flux (kg m^{-2} s^{-1}), w is vertical velocity (m s^{-1}), e and c sub- and super-scripts denote horizontally averaged values conditionally sampled in the cloud environment and core, $forcing$ refers to tracer sources and sinks, such as radiation or subsidence, not included in the other terms, primed values represent anomalies relative to the horizontal mean, overbars represent horizontal averaging, and $E_\phi(z)$ and $D_\phi(z)$ are the total bulk tracer entrainment into and detrainment out of the cloud core in kg s^{-1} m^{-3}.

Alternatively, entrainment and detrainment can be calculated directly from the LES velocity and tracer fields. Romps (2010) recently presented a technique to measure entrainment and detrainment in this manner. His equation (2) is:

$$e - d = \frac{\partial}{\partial t}(\mathcal{A}\rho) + \nabla\cdot(\rho\mathbf{u}\mathcal{A}) \tag{3}$$

Here $e(x,y,z)$ and $d(x,y,z)$ are the local entrainment and detrainment through the cloud core surface in kg s^{-1} m^{-3}, $\mathbf{u}$ is the velocity of the air in m s^{-1}, and $\mathcal{A}$ is the "activity" of

the fluid, where $\mathcal{A}$ is one at "active" cloud core points and zero otherwise. The values of $e - d$ are averaged over the time that a grid cell experiences mass fluxes between an active and an inactive point, then positive $e - d$ values are considered to be purely e, and negative values, d. Summing these point measurements horizontally gives $E_d(z)$ and $D_d(z)$, the total directly calculated cloud core entrainment and detrainment in kg s^{-1} m^{-3}.

Romps found that direct measurement of the fluxes produced values roughly twice as large as tracer budget calculations. Romps attributed this difference to the bulk tracer calculation assumption that fluid exchanged between clouds and environment has the mean properties of the cloud or environment, respectively. The unlikeliness of this assumption is suggested by recent studies of the dense, descending shell of moist air that forms around trade-wind cumulus clouds (Heus and Jonker 2008; Wang and Geerts 2010). Since fluid exchanges between clouds and environment must pass through this shell, it is likely that it plays an important role in entrainment and detrainment dynamics.

Reconciling the direct flux and bulk tracer calculations is important if direct flux calculations are to inform GCM parameterizations. Here we examine the sources of the discrepancy between the methods. We show the discrepancy is explained by three effects: the presence of the moist shell, correlations between the entrainment rates and the tracer values which cause Reynolds fluxes, and numerical errors in the calculation methods. We derive a correction to convert between "tracer" and "direct" entrainment fluxes, and then use this correction to evaluate the impact of variability in the moist shell on bulk tracer entrainment and detrainment rates.

2. Model description

All LES calculations in this paper were made using the System for Atmospheric Modeling (SAM; Khairoutdinov and Randall 2003). Two model runs were performed, configured as standard Global Energy and Water Cycle Experiment (GEWEX) Cloud System Studies (GCSS; Randall et al. 2003) experiments: a Barbados Oceanographic and Meteorological Experiment (BOMEX; Siebesma et al. 2003) run, and an Atmospheric Radiation Measurement Study (ARM; Brown et al. 2002) run. The BOMEX run was performed on a 6.4 km x 6.4 km horizontal x 3.2 km vertical domain with 25 meter grid resolution in all directions for 6 hours, and the first three hours of simulation were discarded. The ARM run was performed on a 7.68 km x 7.68 km x 4.5 km domain with 30 meter grid resolution.

We have implemented the entrainment calculation scheme of Romps (2010) in SAM, allowing us to calculate cloud core entrainment and detrainment directly from model mass fluxes. Romps (2010, eq. 4) also presents a method for calculating tracer entrainment rates in the same framework as (3), but neglects forcing and diffusion terms. These are significant for tracer quantities like vertical momentum, so we retain these terms in Romps's tracer equation:

$$e\phi - d\phi = \frac{\partial}{\partial t}(\phi \mathcal{A}\rho) + \nabla \cdot (\phi \rho \mathbf{u} \mathcal{A}) - \mathcal{A} S_\phi \tag{4}$$

where S_ϕ is any non-advective source term for ϕ, in units of $[\phi]$ s^{-1}. This equation is then averaged in the same way as equation (3), but since ϕ can be negative, negative entrainment fluxes are now possible. If the average value of ϕ over the period of flux averaging is positive, then positive $e\phi - d\phi$ values are considered to be purely $(e\phi)(x, y, z)$, and negative values, $(d\phi)(x, y, z)$. However, if ϕ is negative then positive $e\phi - d\phi$ values are considered to be purely

$(d\phi)(x, y, z)$, and negative values, $(e\phi)(x, y, z)$. Horizontal summation then gives $(E\phi)_d(z)$ and $(D\phi)_d(z)$, the total directly calculated tracer entrainment and detrainment for the cloud ensemble in $[\phi]$ kg s^{-1} m^{-3}.

3. The Cloud Shell

To quantify the effect of the moist cloud shell on entrainment and detrainment we define average or effective tracer values $\phi_E = (E\phi)_d/E_d$ and $\phi_D = (D\phi)_d/D_d$. Examination of these values from the BOMEX simulation using total specfic humidity shows significant differences between q_E and the environmental q_t and between q_D and the core q_t (Figure 1a), confirming that q_E and q_D differ from the mean environment and core values.

Calculated q_D agrees well with the mean "cloud core edge" (cloud core model grid cells that are nearest-neighbor adjacent to non-core cells) q_t values. q_E, however, is moister than the mean "cloud core shell" (non-core model grid cells that are nearest-neighbor adjacent to core cells) values. This suggests that non-trivial Reynolds fluxes exist between q_E and e: more entrainment occurs when q_t is larger than the mean q_t of the shell air, and less when q_t is smaller.

a. E and D correction

Here we derive a correction to equations (1) and (2) to account for the presence of the moist cloud shell and dry cloud edge, allowing us to convert between (E_d, D_d) and (E_ϕ, D_ϕ).

We start our derivation by modifying equation (5.1) from Siebesma and Cuijpers (1995):

$$\rho\frac{\partial a\phi_c}{\partial t} = -\frac{\partial M_c\phi_c}{\partial z} + E_d\phi_E - D_d\phi_D - \frac{\partial \rho a\overline{w'\phi'}^c}{\partial z} + a\rho\left(\frac{\partial\bar{\phi}}{\partial t}\right)_{forcing} \tag{5}$$

$$\rho\frac{\partial(1-a)\phi_e}{\partial t} = \frac{\partial M_c\phi_e}{\partial z} - E_d\phi_E + D_d\phi_D - \frac{\partial \rho(1-a)\overline{w'\phi'}^e}{\partial z} + \rho(1-a)\left(\frac{\partial\bar{\phi}}{\partial t}\right)_{forcing}. \tag{6}$$

Here we have replaced ϕ_e in the entrainment term with ϕ_E and ϕ_c in the detrainment term with ϕ_D, where ϕ_E and ϕ_D are the bulk tracer value of the air being entrained and detrained, respectively.

Next we substitute into (5) and (6) the continuity equation for a cloud plume,

$$\rho\frac{\partial a}{\partial t} + \frac{\partial M_c}{\partial z} = E_d - D_d, \tag{7}$$

allowing us to write

$$E_d(\phi_c - \phi_E) - D_d(\phi_c - \phi_D) = M_c\frac{\partial\phi_c}{\partial z} + \frac{\partial \rho a\overline{w'\phi'}^c}{\partial z} + \rho a\frac{\partial\phi_c}{\partial t} - a\rho\left(\frac{\partial\bar{\phi}}{\partial t}\right)_{forcing} \tag{8}$$

$$D_d(\phi_D - \phi_e) - E_d(\phi_E - \phi_e) = -M_c\frac{\partial\phi_e}{\partial z} + \frac{\partial \rho(1-a)\overline{w'\phi'}^e}{\partial z} + \rho(1-a)\frac{\partial\phi_e}{\partial t} - \rho(1-a)\left(\frac{\partial\bar{\phi}}{\partial t}\right)_{forcing}. \tag{9}$$

Finally, we substitute in equations (1) and (2) for the bulk tracer tendency terms and rearrange to get

$$E_\phi = E_d - E_d\frac{\phi_E - \phi_e}{\phi_c - \phi_e} - D_d\frac{\phi_c - \phi_D}{\phi_c - \phi_e} \tag{10}$$

$$D_\phi = D_d - D_d\frac{\phi_c - \phi_D}{\phi_c - \phi_e} - E_d\frac{\phi_E - \phi_e}{\phi_c - \phi_e}. \tag{11}$$

Note that under this correction $E_d - D_d = E_\phi - D_\phi$, preserving mass continuity.

Comparison of E_{q_t} and D_{q_t} (E_ϕ and D_ϕ inferred using specific humidity q_t as the bulk tracer) with E_d and D_d calculated by the method of Romps (2010) shows the directly calculated values are significantly larger than the bulk tracer values (Figure 1, b and c). Correcting

E_d and D_d using the mean q_t of the cloud core edge and shell in place of q_E and q_D in equations (10) and (11) improves the agreement with the bulk tracer calculations. Relative to the bulk tracer calculation, the corrected E_{q_t} values are still too large near cloud base. However, the correction does duplicate the negative D_{q_t} values near cloud base that are typically produced by bulk tracer calculations.

Including the effect of Reynolds correlations by using $q_E = (Eq_t)_d/E_d$ and $q_D = (Dq_t)_d/D_d$ decreases the corrected E_d and D_d values even further (Figure 1, b and c). This reduces the correction agreement with the bulk tracer calculation over most of the cloud layer, but also reduces the large entrainment values near cloud base, improving the overall shape of the fluxes. Still, the entrainment values corrected by q_E and q_D are about half the magnitude of the Siebesma bulk tracer values.

This overcorrection is the result of numerical errors due to the discrete grid on which the LES fluxes are calculated. To show this, we use alternate equations for the calculation of bulk tracer entrainment and detrainment, derived by Romps (2010):

$$E_\phi(\phi_c - \phi_e) = \phi_c(E_d - D_d) - ((E\phi)_d - (D\phi)_d) \tag{12}$$

$$D_\phi(\phi_c - \phi_e) = \phi_e(E_d - D_d) - ((E\phi)_d - (D\phi)_d) \tag{13}$$

Note that by substituting $(E\phi)_d = E_d\phi_E$ and $(D\phi)_d = D_d\phi_D$ into (12) and (13), we can quickly recover (10) and (11). Because of this, the Romps bulk tracer formulation agrees exactly with the result of the q_E and q_D correction, producing smaller E_{q_t} and D_{q_t} values than the Siebesma bulk tracer calculation.

Siebesma's bulk tracer calculation estimates vertical tracer fluxes from the mean profiles of tracer quantities, while Romps' calculation finds the flux for each grid cell directly from

the numerical model's advection code. Romps' calculation is therefore much more consistent with the model formulation than Siebesma's. Conversely, Romps' calculation requires finding the difference of two large quantities ($\phi_c(E_d - D_d)$ and $(E\phi)_d - (D\phi)_d$), with all the numerical problems that implies. Both these calculation methods therefore are subject to numerical errors that reduce their accuracy.

b. h, w, and Reynolds correlations

Since Reynolds correlations between e and q_t appear to have an important effect on the measured moisture fluxes between cloud and environment, we now examine energy fluxes, represented in SAM by the liquid water moist static energy h (units of J kg^{-1}) and the vertical momentum, represented in SAM by the vertical velocity w (units of m s^{-1}).

Liquid water moist static energy shows a similar distribution of core, edge, shell, environment, h_E and h_D properties when compared to q_t, indicating a tight coupling between these variables in the cloud dynamics (Figure 2a). Near cloud base, edge, shell, h_E and h_D all converge on the core value, spreading out in the cloud layer and becoming relatively more core-like in the inversion. h_D is identical to the edge properties, while h_D is smaller than h in the shell, indicating the influence of Reynolds flux correlations between e and h.

We can quantify the effect of these Reynolds fluxes by looking at $A = (h_E - h_e)/(h_c - h_e)$ and $B = (h_c - h_D)/(h_c - h_e)$, the correction factors in equations (10) and (11). Using the edge and shell values of h for h_E and h_D shows A to have a much larger effect than B, due to the larger difference between the shell and the environment than between the edge and the core. E_d is reduced by 0.2 by the A correction, while 0.45 of D_d is removed by B. If instead

we use $h_E = (Eh)_d/E_d$ and $h_D = (Dh)_d/D_d$ in equations (10) and (11), A is unchanged but B increases to 0.6. Calculations for q_t values show nearly identical results (not shown).

Vertical velocity shows very different relative profiles compared to q_t and h. There is a much wider spread in the w values, with the shell having nearly zero vertical velocity and the edge being halfway between the core and the environment. w_D is again similar to the value of w in the edge, but w_E is much larger than w in the shell, and in fact is roughly the same value as w_D over most of the cloud layer. This large positive value for w_E is clearly inconsistent with the assumption made in many entraining plume models that fluid entrained into the cloud core plume has negligible vertical momentum (Simpson and Wiggert 1969; Gregory 2001; Siebesma et al. 2003)

These differences indicate that Reynolds correlations are much more important to the w fluxes than the q_t or h fluxes. Indeed, using the value of w in the shell to calculate term A results in a value of only about 0.2, while using w_E increased A to 0.45. Term B shows much less sensitivity to the Reynolds fluxes, but is still reduced by about 0.1 by substituting w_D for the edge value of w.

c. Instantaneous Fields

The source of these Reynolds fluxes, and the reason they affect w more than q_t or h, can be seen by comparing instantaneous snapshots of the model values e, e_{q_t}, and e_w. Since Romps (2010) method of calculating e and d requires long time averages over the period that the cloud surface is adjacent to a grid cell, it is unfortunately unsuitable for calculating instantaneous fields. Instead, we use an alternative method we have devised that substitutes

spatial interpolation for time averaging (Dawe and Austin 2011). This alternative method results in slightly smaller values of e and d than are produced by Romps' method, but the two calculations show good agreement in variability. eq_t and ew are calculated simply by multiplying the value of e by the values of q_t and w, respectively.

Examination of these fields shows that, while e and eq_t have a very similar spatial pattern, ew is concentrated in regions where strong updrafts enter the cloud core (Figure 3). The reason for this can been seen by examining the buoyancy, condensed liquid water, and vertical velocity fields that define the cloud core. Of these three fields, buoyancy is the strongest constraint on the core. However, regions exist far above cloud base where air has become negatively buoyant but maintains upward velocity and elevated moisture. As this air continues to rise more condensation occurs, which heats the updraft, makes it positively buoyant, and thus entrains it into the core. In this way, entrainment is positively correlated with both q_t and w. This process occurs fairly often in our model cloud field, as evidenced both by our manual examination of the output fields, and the size of the Reynolds flux terms in the mean profiles.

d. Shell Variability

Finally we ask whether variability of the shell and edge properties has an impact on the measured variability in the bulk tracer calculations of E and D. To do this we turn to the ARM run, and simply look at the variability in $A = (q_E - q_{t_e})/(q_{t_c} - q_{t_e})$ and $B = (q_{t_c} - q_D)/(q_{t_c} - q_{t_e})$. These quantities indeed show strong variability over the ARM diurnal cycle (Figure 4). Near cloud base and within the inversion, A is nearly one while B

is nearly zero. As the clouds mix into the inversion over the course of the day, the values evolve until at mid-cloud layer, A has values near 0.6 and B near 0.2. Performing this calculation with a fixed value of $(q_{t_c} - q_{t_e})$, to remove changes due to movement of the mean environment and core profiles, shows similar results. The shell is clearly an active player in the entrainment and detrainment fluxes.

4. Discussion and Conclusion

We have explained the differences between entrainment and detrainment values calculated via bulk tracer budgets and direct flux calculations by taking into account the properties of the cloud shell, the effect of Reynolds fluxes, and differences in the numerical methods used by the two calculations. This suggests that the presence of the moist cloud shell has a significant role in mediating fluxes between the clouds and the environment and may be an important factor in improving parameterizations of shallow convection.

Significant Reynolds fluxes are apparent in tracer and vertical momentum entrainment. These fluxes are the result of vertical advection of moist but negatively buoyant air so that condensation causes latent heating, making the air buoyant and entraining it into the core. However, this process is not unique to the definition of cloud core. Similar correlations appear when we perform these calculations for regions of condensed liquid water, as vertical advection can drive cloud condensation and thus cause entrainment.

Whether one considers the bulk tracer or directly calculated flux values to be "correct" will depend on the purpose for which they are used. The bulk tracer values are well suited to calculating fluxes in GCM sub-grid scale parameterizations, which only have access to large-

scale values. The influence of variability in the cloud shell would then simply be incorporated into the parameterization of the bulk tracer entrainment and detrainment values. On the other hand, direct fluxes may be needed for calculating fluxes of aerosols whose chemical properties are altered by reactions in the presence of liquid water (Hoppel et al. 1994).

Acknowledgments.

Support for this work was provided by the Canadian Foundation for Climate and Atmospheric Science through the Cloud Aerosol Feedback and Climate network. We thank Marat Khairoutdinov for making SAM available to the cloud modeling community. All figures were generated using the matplotlib library in the Python programming language.

REFERENCES

Bechtold, P., M. Koehler, T. Jung, F. Doblas-reyes, M. Leutbecher, M. J. Rodwell, F. Vitart, and G. Balsamo, 2008: Advances in simulating atmospheric variability with the ECMWF model: From synoptic to decadal time-scales. *Q. J. R. Meteorol. Soc.*, **134 (634, Part A)**, 1337–1351, doi:10.1002/qj.289.

Brown, A. R., et al., 2002: Large-eddy simulation of the diurnal cycle of shallow cumulus convection over land. *Q. J. R. Meteorol. Soc.*, **128**, 1075–1093.

Dawe, J. T. and P. H. Austin, 2011: Interpolation of LES cloud surfaces for use in direct calculations of entrainment and detrainment, submitted to Monthly Weather Review.

de Rooy, W. C. and A. P. Siebesma, 2010: Analytical expressions for entrainment and detrainment in cumulus convection. *Q. J. R. Meteorol. Soc.*, **136 (650)**, 1216–1227, doi: 10.1002/qj.640.

Gregory, D., 2001: Estimation of entrainment rate in simple models of convective clouds. *Q. J. R. Meteorol. Soc.*, **127 (571, Part A)**, 53–72.

Heus, T. and H. J. J. Jonker, 2008: Subsiding shells around shallow cumulus clouds. *J. Atmos. Sci.*, **65**, 1003–1018.

Hoppel, W. A., G. M. Frick, J. Fitzgerald, and R. E. Larson, 1994: Marine boundary-layer measurements of new particle formation and the effects nonprecipitating clouds have on aerosol-size distribution. *J. Geophys. Res.-Atmos.*, **99**, 14 443–14 459.

Khairoutdinov, M. F. and D. A. Randall, 2003: Cloud resolving modeling of the arm summer 1997 iop: model formulation, results, uncertainties, and sensitivities. *J. Atmos. Sci.*, **60**, 607–625.

Randall, D., et al., 2003: Confronting models with data: The GEWEX cloud systems study. *Bulletin of the American Meteorological Society*, **84 (4)**, 455–469, doi:10.1175/BAMS-84-4-455, URL `http://journals.ametsoc.org/doi/abs/10.1175/BAMS-84-4-455`, `http://journals.ametsoc.org/doi/pdf/10.1175/BAMS-84-4-455`.

Romps, D. M., 2010: A direct measure of entrainment. *J. Atmos. Sci.*, **67 (6)**, 1908–1927.

Rougier, J., D. M. H. Sexton, J. M. Murphy, and D. Stainforth, 2009: Analyzing the climate sensitivity of the HADSM3 climate model using ensembles from different but related experiments. *J. Climate*, **22 (13)**, 3540–3557, doi:10.1175/2008JCLI2533.1.

Siebesma, A. P. and J. W. M. Cuijpers, 1995: Evaluation of parametric assumptions for shallow cumulus convection. *J. Atmos. Sci.*, **52**, 650–666.

Siebesma, A. P., et al., 2003: A large eddy simulation intercomparison study of shallow cumulus convection. *J. Atmos. Sci.*, **60 (10)**, 1201–1219.

Simpson, J. and V. Wiggert, 1969: Models of precipitating cumulus towers. *Mon. Wea. Rev.*, **97 (7)**, 471.

Wang, Y. and B. Geerts, 2010: Humidity variations across the edge of trade wind cumuli: Observations and dynamical implications. *Atmos. Res.*, **97 (1-2)**, 144 – 156, doi:DOI:10.1016/j.atmosres.2010.03.017, URL `http://www.sciencedirect.com/science/article/B6V95-4YPPPTH-2/2/7398151adf50038f1b76265010f57c38`.

List of Figures

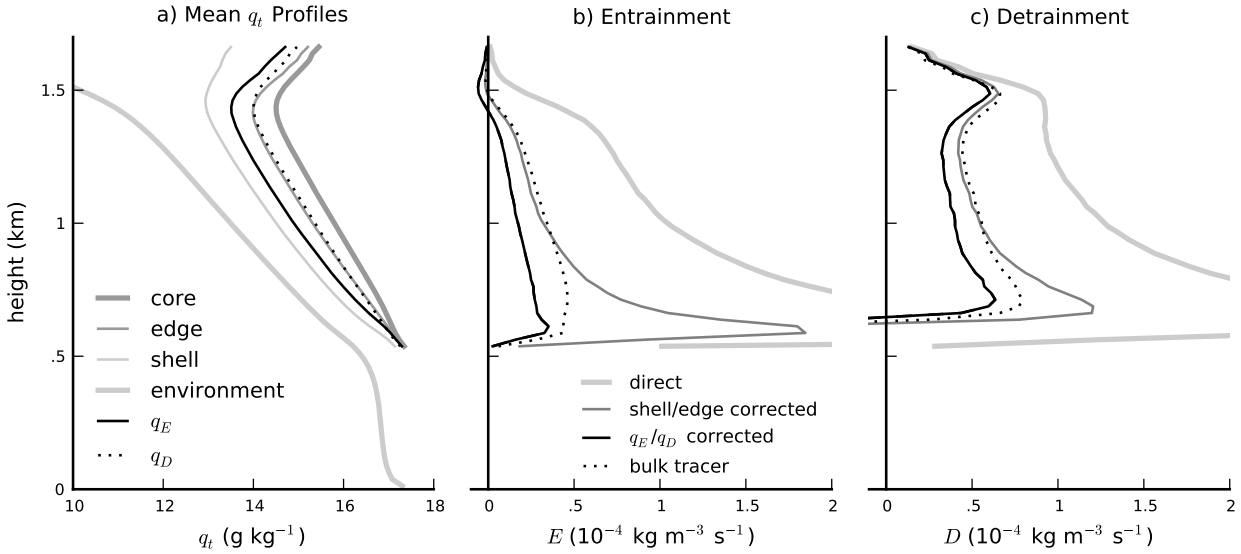

FIG. 1. Result of correcting direct entrainment values for the presence of the moist cloud shell. a) Mean profiles of the effective total specific humidity values being entrained (q_E, black line), and detrained (q_D dotted line), overlaid on the total specific humidity in the cloud core (thick dark grey line), cloud core edge (thin dark grey line), cloud core shell (thin grey line), and cloud core environment (thick grey line). These q_t values are used to correct values of b) entrainment and c) detrainment; shown are the direct flux calculation of Romps (2010) (thick grey line), the bulk tracer budget calculation of Siebesma and Cuijpers (1995) (dotted line), the direct flux calculation corrected by the mean core shell and edge values ("shell/edge corrected", thin grey line), and the direct flux calculation corrected by the q_E and q_D values ("q_E/q_D corrected", black line).

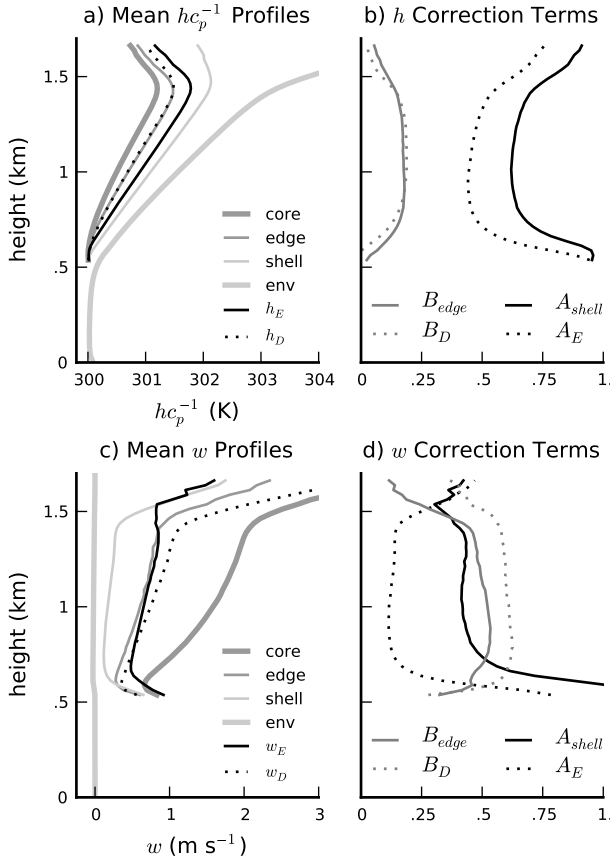

FIG. 2. Mean profiles of a) liquid-water moist static energy values for entraining (black line) and detraining (dotted line) air, overlaid on the mean core, edge, shell, and environment profiles (grey lines), and b) the resulting $A_{shell} = (h_{shell} - h_e)/(h_c - h_e)$, $A_E = (h_E - h_e)/(h_c - h_e)$, $B_{edge} = (h_c - h_{edge})/(h_c - h_e)$, and $B_D = (h_c - h_D)/(h_c - h_e)$ profiles. c) and d) are the same as a) and b), but calculated for w.

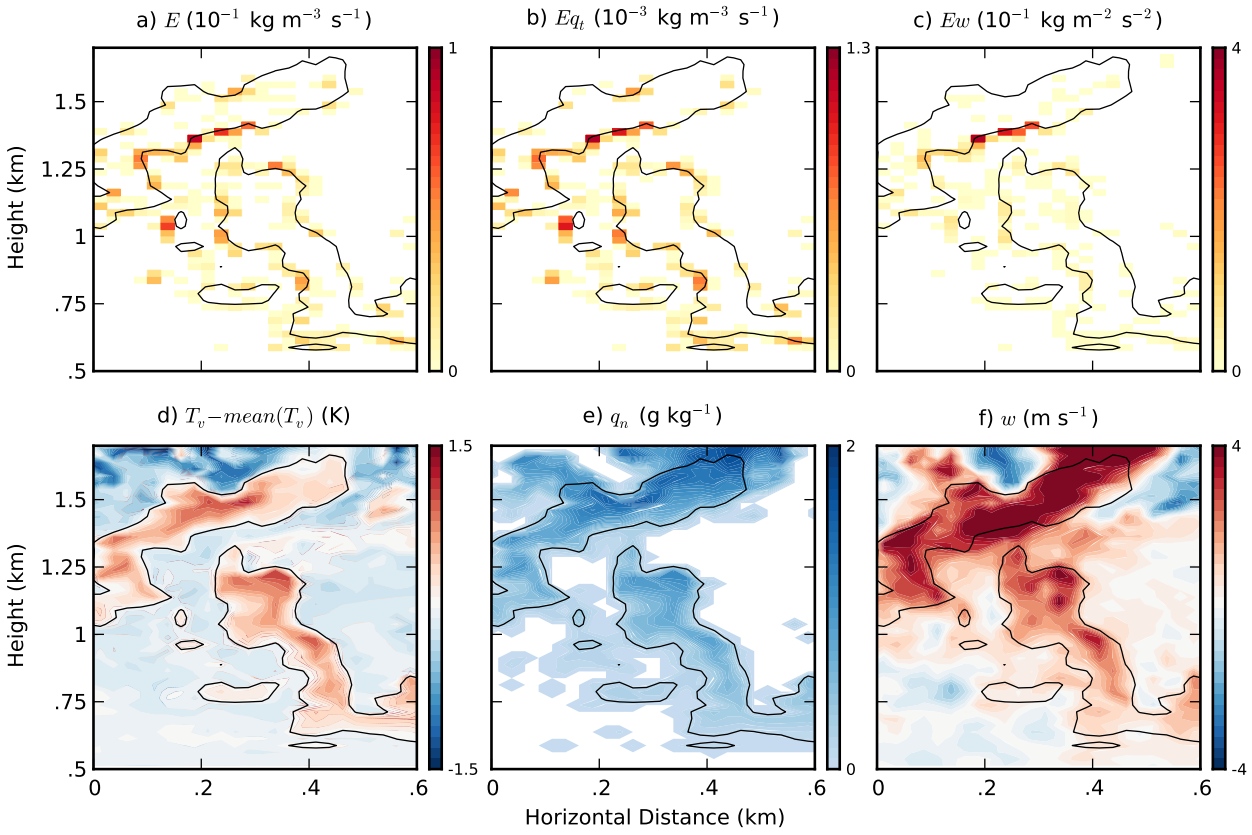

FIG. 3. Instantaneous vertical cross-section of cloud core mass entrainment (a), humidity entrainment (b), vertical velocity entrainment (c), buoyancy (d), condensed liquid water (e), and vertical velocity (f) of a single model cloud, illustrating the Reynolds correlation between vertical velocity and entrainment. Black lines indicate the edge of the cloud core in each figure.

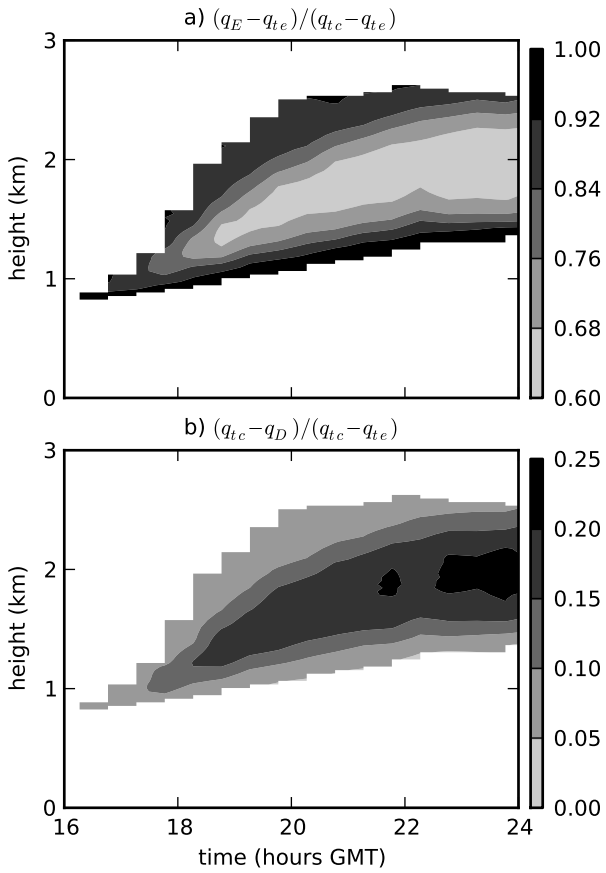

FIG. 4. Variation in a) $(q_E - q_{te})/(q_{tc} - q_{te})$ and b) $(q_{tc} - q_D)/(q_{tc} - q_{te})$ over the duration of the ARM model run.